Spring 5-6-2020

Raman Spectroscopy Study of Delta-9-Tetrahydrocannabinol and Cannabidiol and their Hydrogen-Bonding Activities

Kalee Sigworth

Raman Spectroscopy Study of Delta-9-Tetrahydrocannabinol and Cannabidiol and their Hydrogen-Bonding Activities

By

Kalee Noelle Sigworth

A thesis submitted to the faculty of The University of Mississippi in partial fulfillment of the requirements of the Sally McDonnell Barksdale Honors College.

Oxford

May 2020

Approved By:

Dr. Nathan Hammer

Advisor

Dr. Robert Doerksen

Reader

Dr. Murrell Godfrey

Reader

ACKNOWLEDGEMENTS

This work has been supported, in part by the National Science Foundation and by the University of Mississippi. I would first like to thank my parents for providing me with the opportunity to attend the University of Mississippi and for supporting me throughout my experience here. I would also like to thank the University of Mississippi's Department of Chemistry and Biochemistry for challenging me in my undergraduate years. I am also grateful to the University of Mississippi Department of BioMolecular Sciences for providing me with resources to complete my thesis to the fullest capacity under the conditions. Finally, I would like to thank Dr. Nathan Hammer and the Hammer Research Group. Dr. Hammer remained incredibly positive and was a guiding figure throughout my experience. He and the graduate students in the Hammer Group taught me innumerable things that I will carry with me into future endeavors.

ABSTRACT

KALEE NOELLE SIGWORTH: "Raman Spectroscopy Study of Delta-9-Tetrahydrocannabinol and Cannabidiol and their Hydrogen-Bonding Activities"

(Under the direction of Dr. Nathan Hammer)

Cannabis and products containing its cannabinoids have grown rapidly in acceptance and use in recent years with legalization of cannabis in many countries and US states. Cannabidiol and Delta-9-Tetrahydrocannabinol are two primary cannabinoids in Cannabis that have been shown to produce analgesic effects along with many other positive side effects for the user. These two cannabinoids interact with receptors in the Central and Peripheral Nervous Systems. No spectroscopic study to our knowledge has been performed to analyze the hydrogen bonding effects of interactions between these two cannabinoids and solvents. Here, we employ theoretical Raman spectra through computational methods to study hydrogen bonding between cannabinoids and water, ethanol and methanol. Additionally, computational chemistry was utilized in an effort to identify the lowest energy conformations of Delta-9-THC and CBD in the presence of solvents. Experimental Raman spectroscopy was also applied in an effort to acquire the highest resolution Raman spectra ever recorded for CBD and Delta-9-THC to date. Due to the COVID-19 pandemic, experimental work was limited and will likely be completed in future work.

TABLE OF CONTENTS

LIST OF FIGURES

LIST OF ABBREVIATIONS

Δ^9-THC / Delta-9-THC: Delta-9-Tetrahydrocannabinol

CBD: Cannabidiol

ECS: Endocannabinoid System

CNS: Central Nervous System

PNS: Peripheral Nervous System

FAAH: Fatty Acid Amide Hydrolase

THCA: Tetrahydrocannabinolic acid

NMR: Nuclear Magnetic Resonance

CCD: Charge-Coupled Device

LCAO: Linear Combination of Atomic Orbitals

SERS: Surface Enhanced Raman Spectroscopy

HF: Hartree-Fock

DFT: Density Functional Theory

SCF: Self Consistent Field

B3LYP: Becke 3-Parameter, Lee, Yang, Parr

Gr/mm: Grooves per millimeter

Chapter 1: Introduction to Chemical Bonding & Cannabinoids

1.1. Chemical Bonds

The most basic understanding of chemical processes and reactions depends upon an understanding of chemical bonding. Essentially all molecules exist as a result of atomic bonding to create molecules or chemical reactions. Individual atoms are composed of a nucleus containing positively charged protons and neutrons possessing no charge. Floating freely around the nucleus are negatively charged electrons that participate in bonding. Chemical bonds occur if the bonded state is lower in energy and therefore more favorable than the free atom state. The properties of chemical bonds are heavily dependent on the atoms they connect and their electronic interactions. Covalent bonding involves the sharing of electrons between atoms and occurs between two nonmetals seeking to fill their valence subshells. Covalent bonds can be polar or nonpolar, depending on the difference in electronegativities of the participating atoms. Electronegativity can be defined as the ability of an atom to attract electrons to itself within a molecule [1]. An example a polar covalent molecule is water, as shown in **Figure 1.1**. Due to oxygen's stronger ability to attract electron density, its electronegativity is significantly greater than hydrogen's. Polar covalent bonds create partial dipole moments between atoms participating in the bond caused by unequal sharing of electron density. In **Figure 1.1**, the oxygen possesses a partial negative charge due to lone pairs of electrons and strong electronegativity. Both hydrogens possess a partial positive charge, as they lack electron density and their charge is dominated by their nuclei. Oxygen is able to donate electron density to proximal hydrogens through its lone pairs in a process known as hydrogen bonding which is discussed in **Chapter 1.1.2**. Because water has hydrogens and an electron rich oxygen, it can behave as a hydrogen

bond donator or an acceptor. Hydrogen bond donors are those who donate their hydrogen to accept electron density from an electron rich atom, while hydrogen bond acceptors are the electron rich atoms that accept hydrogens and subsequently donate some of their electron density to the hydrogen. While all bonds are relevant to chemical analysis, the primary interactions of interest here are noncovalent interactions between covalently bonded molecules.

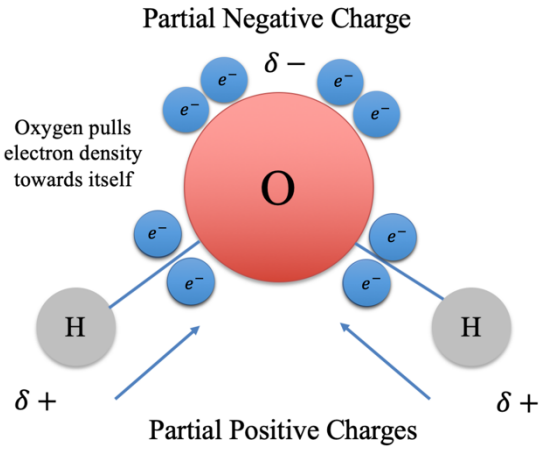

Figure 1.1: *Net dipole moment of water, a result of differences in electronegativity. Adapted from [2]*

1.1.1. Noncovalent Interactions

Noncovalent interactions occur between individual molecules or between different functional groups within the same molecule. Therefore, noncovalent interactions can be intermolecular or intramolecular. These interactions occur due to dipole moments created by unequal sharing of electron density between two atoms. Types of noncovalent interactions include van der Waals forces, ionic interactions and hydrogen bonding interactions. Van der Waals forces commonly occur between nonpolar molecules that are closely-packed. These molecules have a weak but constantly changing dipole moment that with a large number of nonpolar molecules will create a network of dipole moment

interactions. These noncovalent interactions are believed to be the weakest of the three. Additionally, ion-ion interactions involve two ionic atoms or molecules aligning so their oppositely charged dipoles are interacting favorably. Ion-dipole interactions may also occur, but are weaker than ion-ion interactions. The final noncovalent interaction is hydrogen bonding, and is important to understanding the purpose of solvated studies in this work.

1.1.2. Hydrogen Bonding

Hydrogen bonding is a noncovalent interaction resulting from dipole–dipole interactions involving a covalently bound hydrogen and an electronegative atom possessing a lone pair. The polar covalent interaction strips electron density from the hydrogen, allowing a proximal electronegative atom to partially donate its electron density in the form of a lone pair of electrons. No true bonding is occurring between the proximal atom and the hydrogen, but rather overlap of the antibonding orbital of the hydrogen bonded pair with the lone pair orbital of the accepting atom. This allows sharing of electron density, stabilizing both orbitals in the process. An example of hydrogen bonding is provided in **Figure 1.2**, in which the Delta-9-THC displays both intermolecular hydrogen bonding with the water molecule as well as intramolecular hydrogen bonding between the molecule's oxygen and an alkane located near the oxygen's lone pair. The hydrogen bonds are signified by the dashed yellow lines connecting hydrogen and oxygen atoms. In this case, the water is behaving as a hydrogen bond acceptor, by accepting the hydrogen and the phenol group is both an acceptor and donor by donating its hydrogen and accepting a hydrogen from the alkane.

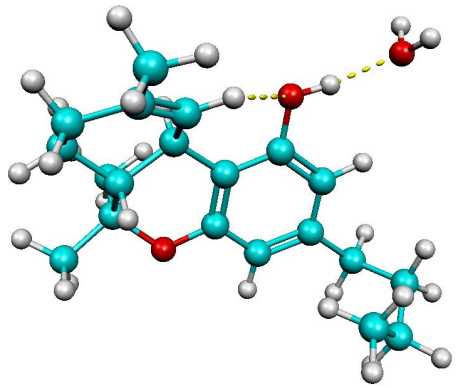

Figure 1.2: *Example of hydrogen bonding in an interaction between Delta-9-THC and water*

Individual hydrogen bonds are relatively weak and therefore easy to break with heat, but most systems contain a large number of hydrogen bonds which have the ability to lower the energy of a total network. An example of this is the hydrogen-bonding properties of liquid water. The existence of hydrogen bonding increases water's boiling point and alters its density and adhesion properties.

1.2. Cannabis

1.2.1. History and Usage

Cannabis sativa and *Cannabis indica* are two species of Cannabis commonly used to produce marijuana products. Marijuana is the dried flowers and leaves of a Cannabis plant. Cannabis has been grown for centuries and used both recreationally and medicinally. In 1937, the federal government passed the Marihuana Tax Act, which effectively criminalized the possession of Cannabis at the federal level [3]. Today, Marijuana is the most commonly used illicit drug in the world [4]. Cannabis is currently a Schedule I drug under federal law, defined as criminally illegal to possess with no accepted medical use in the United States and a high potential for abuse [5]. Despite this federal prohibition, eleven US states have legalized recreational marijuana use and forty-seven US states allow

medicinal marijuana with varying degrees of regulation [6]. Traditionally, Cannabis is used by burning the dried leaves and oral inhalation of smoke. With the increasing acceptance of Cannabis, novel methods of administration have been created, allowing for Cannabis use without producing a distinctive odor. Over five hundred compounds have been identified from the Cannabis plant, with over one hundred of these being cannabinoids, or compounds unique to Cannabis that interact with the endocannabinoid system [7]. Because of their large concentration in Cannabis and recognition by the public, the two cannabinoids of interest in this study are Delta-9-Tetrahydrocannabinol (Δ^9-THC) and Cannabidiol (CBD).

1.2.2. Regulation and Potential Health Risks

The public outlook on Cannabis use continues to change drastically as more states allow its legalization. This change in perspective comes with an increase in public usage as well as potential risks to personal and public health. Overall, the use of Cannabis has become less taboo to the public eye and therefore formal action to regulate the safety of Cannabis products has become a growing necessity in the drug industry. Many new methods of administration have been created such as food products, oils and e-cigarette fluids containing cannabinoids [8]. These new methods often involve the isolation of specific cannabinoids such as Delta-9-THC or CBD to increase their potency. In addition to increased recreational usage, it is likely that with increasing acceptance there will also be an increase in medical applications for cannabinoids, especially for their influence on the Endocannabinoid system.

1.3. The Endocannabinoid System

The Endocannabinoid System (ECS) consists of CB1 and CB2, which are G-protein coupled receptors, along with endocannabinoids, or endogenous lipid compounds, and enzymes [9]. CB1 receptors are heavily concentrated in the Central Nervous System (CNS) but are also distributed throughout the Peripheral Nervous System (PNS) and peripheral tissues. CB2 receptors are primarily distributed throughout the peripheral tissues, with significant concentration in immune tissues [10], [11]. CB1 receptors inhibit neurotransmitter release when activated and this activation can be influenced by both human endocannabinoids and cannabinoids. Delta-9-THC is a CB1 agonist, inhibiting the release of neurotransmitters from a presynaptic neuron. This inhibition of neurotransmitters such as GABA and glutamate are suggested to be the source of Delta-9-THC's depressant nature. Additionally, Delta-9-THC has the ability to selectively behave as an antagonist, stimulating the release of neurotransmitters, the likely origin of Delta-9-THC's psychotropic and euphoric properties [12],[13].

Much less is known about the exact mechanisms in which CBD affects ECS receptors. In fact, it has generally been proposed that CBD has negligible interaction directly with both CB1 and CB2, posing greater benefits with anti-oxidant properties [14]. It has been proposed that CBD inhibits fatty acid amide hydrolase (FAAH), a membrane protein on a postsynaptic cell that works to degrade endocannabinoids [15]. By inhibiting FAAH through preferential binding, high levels of endocannabinoids remain in the tissues which activate CB1 receptors on the presynaptic neuron, inhibiting release of neurotransmitters. Therefore, the study published by the Li group suggests that CBD indirectly activates CB1 function and is therefore a CB1 agonist [15].

1.4. Delta-9-Tetrahydrocannabinol

1.4.1. Structure and Properties

Delta-9-THC has a molecular weight of 314.5 g/mol. Isolated Delta-9-THC is crystalline at room temperature, but becomes an easily vaporable oil upon heating, which contributes to its versatility in use. Delta-9-THC contains two oxygen atoms, one of which exists as a phenol while the other is sequestered in a furan ring, in which it can only behave as a hydrogen bond acceptor. Very little free Delta-9-THC is found in natural Cannabis, yet its chemical precursor, tetrahydrocannabinolic acid (THCA) is abundant [16]. THCA is pharmacologically inactive because it cannot pass the blood brain barrier and will not

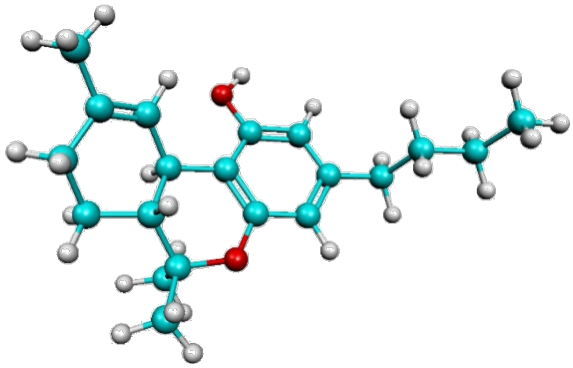

Figure 1.3: *Optimized molecular structure of Delta-9-Tetrahydrocannabinol (Δ^9-THC)*

produce the same pharmacological effects as Delta-9-THC [17]. When Cannabis is heated, a carboxyl group is removed from THCA and Delta-9-THC is produced. Therefore, to measure the total content of Delta-9-THC in a Cannabis sample, analysts must measure both Delta-9-THC and THCA content. Most forensic laboratories utilize Gas Chromatography to isolate cannabinoids from marijuana, a highly accurate method that destroys the sample in the analysis.

1.4.2. Usage and Effects

As introduced previously, Delta-9-THC is primarily responsible for the psychoactive effects of Cannabis. Delta-9-THC metabolizes quickly in the body and can be stored in adipose tissue for weeks after use [18]. Delta-9-Tetrahydrocannabinol is a highly lipophilic substance with poor aqueous solubility [16]. Delta-9-THC behaves to a lesser extent a CB2 agonist. Delta-9-THC has the greatest effects in the CNS where CB1 receptors are most heavily concentrated. Examples of regions possessing a heavy concentration are the cerebral cortex and hippocampus, in which the effects of inhibited memory and cognitive function are produced [19]. Delta-9-THC acts as a CNS depressant, similarly to alcohol, with both depressants having shown effects such as drowsiness and hunger. A primary medicinal effect studies have found suggests Delta-9-THC has analgesic properties, reducing pain and discomfort in users [20]. Prescription Delta-9-THC capsules, such as Dronabinol, have been used for years as an appetite stimulant in AIDS patients and more recently been given to cancer patients experiencing nausea caused by chemotherapy treatments [21]. Despite positive effects reported in studies, Delta-9-THC carries the risk of impairment to motor function, a significant factor contributing to the potential danger of inhibition in daily life.

1.5. Cannabidiol

1.5.1. Structure and Properties

Depending upon the strain of the plant Cannabis is taken from, Cannabidiol accounts for an average of forty percent of the cannabinoid concentration in Cannabis. CBD has the same molecular weight as Delta-9-THC of 314.5 g/mol. The two molecules differ structurally in that Cannabidiol possesses its second oxygen atom as an additional

phenol group, rather than the furan ring in Delta-9-THC. Additionally, Cannabidiol possesses a terminal alkene and the two rings of the molecule are almost perpendicular to each other about a single carbon bond, a result of repulsion between the phenols and the terpene ring. The optimized molecular structure of Cannabidiol is provided below in **Figure 1.4**.

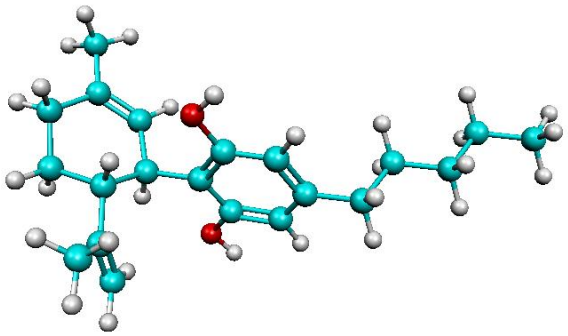

Figure 1.4: *Optimized molecular structure of Cannabidiol (CBD)*

1.5.2. Usage and Effects

Unlike Delta-9-THC, Cannabidiol does not induce psychoactive effects [22]. As early as the 1800s, doctors reported the use of CBD for the successful reduction of epileptic seizures [23]. A study published in 2012 found CBD to produce anti-nausea responses through indirect activation of dorsal raphe nucleus receptors [24]. It is widely believed that CBD provides neuroprotective effects, promoting the clinical use of CBD for improving symptoms of epilepsy and Parkinson's disease [25]. The anticonvulsant drug Sativex®, contains both CBD and Delta-9-THC. CBD has been observed to mediate negative effects of Delta-9-THC while synergistically enhancing the positive effects [26]. Recreational CBD use is legal in most US states and commercial products containing CBD have been primarily marketed towards children, the elderly and patients suffering from more complex illnesses [27]. CBD has also been marketed to the general public as providing analgesic properties yet few studies have shown CBD to produce analgesic

effects. CBD is generally accepted as a dietary supplement that improves neurodegenerative and anxiety conditions, despite significant evidence.

1.6. Solvents Included

The solvent molecules included in the computational study were water, ethanol and methanol, all chosen for specific reasons. Water was chosen because it is abundant in the blood stream and throughout the body, therefore it is nearly impossible for cannabinoids to avoid interaction with water in the body despite their hydrophobic nature. Water may also interact with cannabinoids in Cannabis products, such as vape juices or food products. Ethanol was chosen because of its significance in drinking alcohol, a depressant that is sometimes ingested by individuals in combination with Cannabis. These depressants can produce synergistic effects, commonly referred to as a condition of "cross-fade" [28]. It is possible that interactions directly between cannabinoids and ethanol could play a role in this effect. Biologically, methanol is toxic to humans and therefore does not have relevance to understanding biological interactions of cannabinoids. Despite this, methanol was chosen because it is a common solvent for industrial and commercial samples of Delta-9-THC and Cannabidiol, making it useful to understand interactions for research purposes. Additionally, all of these solvents may potentially alter the Raman spectra of Delta-9-THC or Cannabidiol.

Chapter 2: Spectroscopy

2.1. Electromagnetic Spectrum

Spectroscopy is the study of the absorption, emission or scattering of radiation by matter. The electromagnetic spectrum ranges from Gamma ray radiation of highest energy to radio waves of lowest energy. Because light possesses particle-wave duality, it can be characterized as an oscillating wave with electromagnetic properties as well as a discrete packet of light. Discrete light packets are commonly referred to as photons and are important to understanding spectroscopy methods such as scattering. The energy of light has an inverse relationship to its wavelength, meaning that with increasing wavelength, the energy of the photons decreases, which is elucidated in **Figure 2.1**.

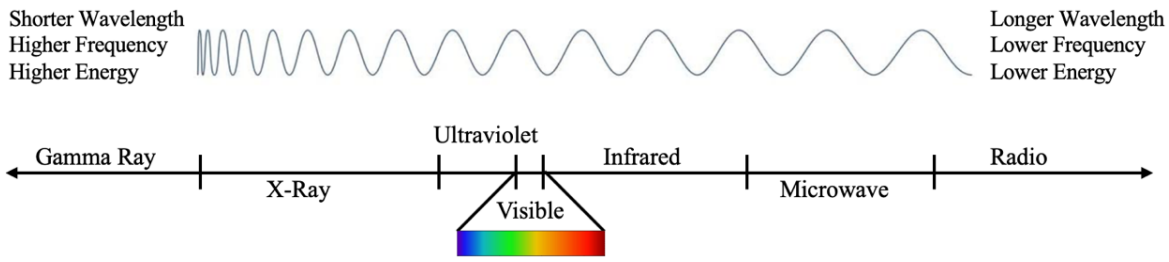

Figure 2.1: *The Electromagnetic Spectrum. Adapted from [29]*

Many methods of spectroscopy exist as a result of incident radiation manipulation, which allow for various properties to be observed in a sample. Gamma rays and X-rays are high energy wave particles often used in the medical field. For example, Gamma rays arise from decay in an atom's nucleus and have the ability to kill living cells, a useful technique for tumor removal. X-rays cause ejection of core electrons from a sample atom and are most commonly used for deep tissue imaging. Following Gamma rays and X-rays is UV-Visible spectroscopy, which causes electronic excitations in conjugated double

bonds. In accordance to Beer-Lambert's Law, UV-Vis allows determination of the concentration of a solvated sample. This law can be written as $A = \varepsilon bc$ where A represents the degree of absorption, ε represents the molar absorptivity, unique to each molecule, b represents path length of a cuvette and c represents concentration of analyte. Raman spectroscopy uses monochromatic visible light to induce light scattering events. Raman spectroscopy was employed in this study and will be discussed further in following sections. Infrared spectroscopy generates absorption of infrared radiation by the analyte, causing bonding vibrations as the molecule is excited. IR spectroscopy is a reliable method that produces spectra for identification of distinct functional groups. Beyond Infrared are microwaves and radio waves, with microwave spectroscopy being lesser recognized and radio waves being vital to the use of Nuclear Magnetic Resonance (NMR) allowing for determination of atomic arrangement within a molecule.

2.2. Vibrational Spectroscopy

2.2.1. Vibrational Motions

There are four energy level transitions that spectroscopic methods induce and analyze. These are Translational, Rotational, Vibrational and Electronic, listed in order of increasing energy and magnitude. Vibrational transitions are the primary focus of this discussion and are analyzed by Infrared spectroscopy and Raman spectroscopy. Vibrational transitions between two bonded atoms cause oscillations in the bonds. For this reason, vibrational motion is understood based upon the simple harmonic oscillator, a model from classical physics representing the oscillatory behavior of a spring. The harmonic oscillator represents bond length between two atoms, where the bottom of its potential energy well represents the most stable, or lowest energy, bond length possible.

The linear restoring force of a harmonic oscillator follows Hooke's Law, which is commonly written as follows.

$$F = -kx \qquad \textbf{(Equation 2.1)}$$

In **Equation 2.1**, F is the force experienced by the object, k is the stiffness of the spring and x is the displacement of the spring by the motion. By this model, the force of the harmonic oscillator is proportional to the displacement where k is a positive constant. Force can also be related to potential energy according to another famous equation in classical physics.

$$F = -dV/dx \rightarrow\rightarrow V = \tfrac{1}{2}*kx^2 \qquad \textbf{(Equation 2.2)}$$

The derivation of **Equation 2.2** creates the harmonic potential energy well which follows a parabolic shape. Despite this ideal model, realistic diatomic vibrational motion follows an anharmonic oscillatory behavior and vibrational states get closer together as they increase in energy. The anharmonic oscillator is dependent on a nonlinear restoring force since the response is dependent upon displacement squared and its shape is not perfectly parabolic. Even though the potential energy well is modeled upon a diatomic molecule, it has relevance in understanding the anharmonic behavior of real molecules. The Morse Potential, shown in red, represents the potential energy well for an Anharmonic Oscillator. This represents the realistic bond activity of a diatomic, suggesting that at some great distance of internuclear separation, the bond breaks. The potential energy well for a Harmonic Oscillator is provided in blue in **Figure 2.2**. As the distance between the nuclei of two atoms gets very small or very large, the energy of both potentials increases exponentially. The difference occurs in the Morse Potential when there is great

internuclear separation between the two atoms, resulting in eventual separation between the two atoms. The energy of the system levels off but does not drop off because the atoms are now separated and partially unstable since their valence shells are no longer filled through bonding.

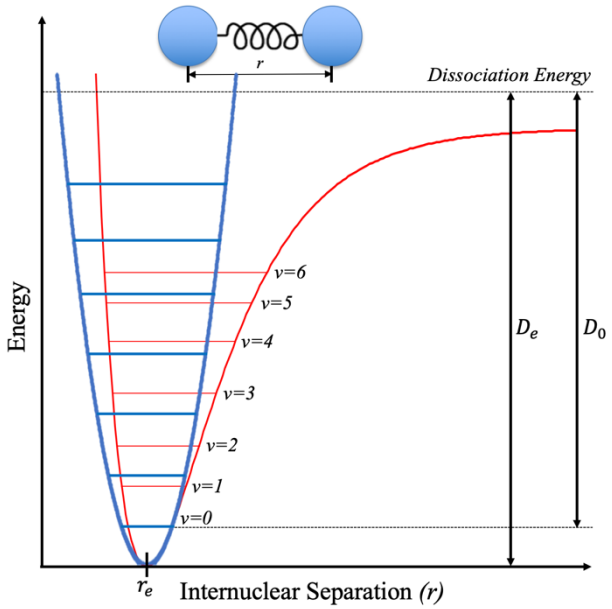

Figure 2.2: *The Harmonic Oscillator potential energy well (blue) and the Anharmonic Oscillator potential energy well (red). Adapted from [30]*

Infrared spectroscopy and Raman spectroscopy produce spectra based on vibrations between bonds and are similar, but possess distinct differences. For a vibrational mode to be active in Infrared spectroscopy, there must be a change in the net dipole moment during the vibration. Infrared spectroscopy exploits absorption of Infrared radiation, which is invisible to the human eye and lower in energy than the visible, monochromatic light used in Raman spectroscopy. Raman spectroscopy analyzes scattering events and Raman active modes possess a net change in polarizability during a vibration. Because Raman and IR have different selection rules, some vibrational modes are Raman active and IR inactive or vice versa. Additionally, Raman spectroscopy dominates in the analysis of aqueous solutions because water is Raman inactive but a strong infrared absorber, overwhelming

the IR spectrum. Both techniques are useful for analyzing the vibrational frequencies of various molecules.

2.3. Raman Spectroscopy

2.3.1. Theory and Instrumental Design

The phenomena behind Raman spectroscopy was discovered by C. V. Raman in 1928 using simple instrumentation and Raman's own eyesight as a detector [31]. This phenomenon, the Raman Effect, is the study of the small fraction of detected light different in frequency and wavelength from the incident light. This is a result of interaction between the sample molecules and incident light causing light scattering [32]. Therefore, Raman spectroscopy is a measure of the degree of light scattering resulting from light and matter interactions. The degree of light scattering is referred to as a Raman shift, measured in wavenumbers, or inverse wavelength in centimeters. Three light scattering events may occur in a Raman analysis and are categorized as either inelastic or elastic scattering. These are Rayleigh scattering, Stokes Raman scattering and Anti-Stokes Raman scattering, listed in order of likelihood to occur and illustrated in **Figure 2.3**. Rayleigh scattering is elastic scattering of light where no energy is lost or gained by the photon after sample interaction. Rayleigh scattering is the most common scattering event but is not useful in Raman spectroscopy. Stokes Raman scattering is the most commonly occurring inelastic scattering event and is vital to Raman analysis. Incident light transfers energy to the sample, exciting the sample to a virtual state and returning to the detector lower in energy. Anti-Stokes inelastic scattering is less likely because incident light gains energy from

sample interaction. This may occur if the sample were excited to a virtual state prior to interaction, a potential result of heating or being especially unstable.

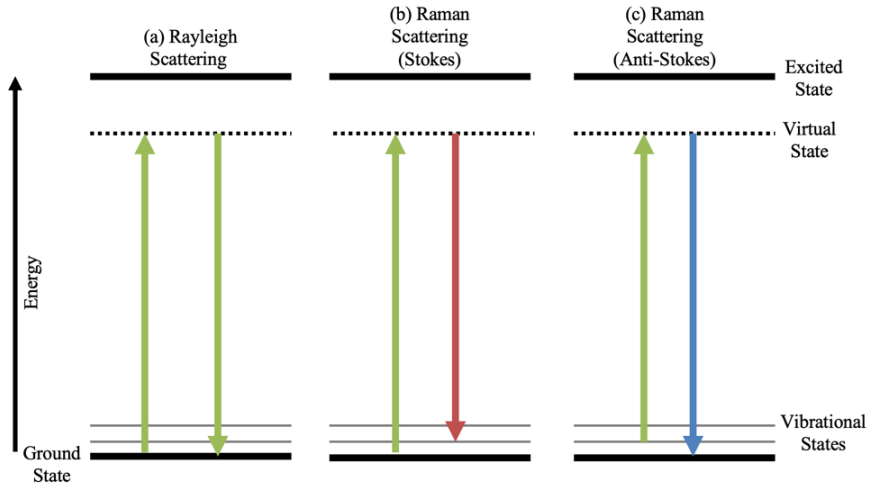

Figure 2.3: *Light scattering events in Raman spectroscopy. Adapted from [33]*

It is estimated that one in every million photons interacting with a sample will produce inelastic scattering, making Raman spectroscopy difficult if a sample does not possess many Raman active modes. As previously discussed, a vibrational mode must possess a net change in polarizability during the vibrational motion to be Raman active. Polarizability is the ability of a bond to form dipole moments instantaneously and is a common property of polar covalent bonds. The amount of total vibrational modes that can be observed by a nonlinear molecule is determined by the following formula where N represents the number of atoms in a given molecule. For example, according to **Equation 2.3,** a molecule of Delta-9-THC is expected to possess 153 vibrational modes because it contains fifty-three atoms. Not all vibrational modes are Raman active because not all vibrations follow the selection rule, so fewer vibrational modes are observed than calculated from **Equation 2.3**.

Vibrational Modes for Nonlinear Molecule = 3N – 6 (**Equation 2.3**)

Figure 2.4 represents intramolecular motions that may be observed in Vibrational spectroscopy. There are two primary categories of vibrational motion which are stretching and bending. Stretching refers to the symmetric or antisymmetric stretching of bonds while bending is the motion of bonded atoms relative to a central atom.

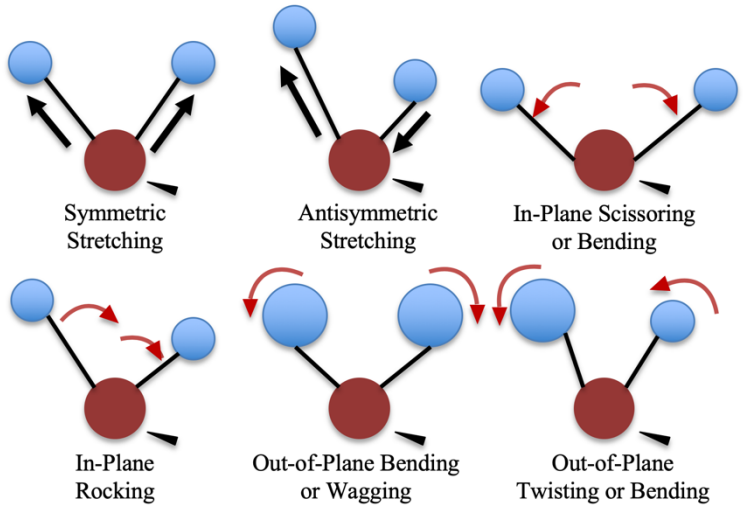

Figure 2.4: *Potential vibrational modes in a nonlinear molecule. Adapted from [34]*

Raman spectrometers may have various orientations but consist of the same necessary components. There must be a monochromatic light source to produce excitation, in which a laser is commonly used. Laser stands for Light Amplification by Stimulated Emission of Radiation. Increasing the frequency of incident radiation through use of a different laser increases Raman intensity but risks overwhelming Raman signals by fluorescence. On the other hand, if the incident radiation is too low in energy, the photons may not be able to excite the sample to a virtual state, producing no Raman spectrum. Raman spectrometers also contain lenses which can block particular wavelengths from reaching the detector or focus the beam. The laser excites the sample to a virtual state and resulting light scattering is then narrowed through a slit. It is very important to focus the

beam of photons because Raman signals are inherently weak and it is in the analyst's best interest to increase resolution of scattering events. The narrow beam of light hits a diffraction grating which has grooves that separate the beam into a spectrum which can be detected by a CCD camera. The Charge Coupled Device (CCD) detector then sends the signal to a computer software program which produces a Raman spectrum from the data. CCD detectors are highly sensitive and can detect a full spectrum in a single acquisition, making them a common detector used in Raman spectroscopy. **Figure 2.5** is a schematic of the inside of a LabRAM Raman spectrometer.

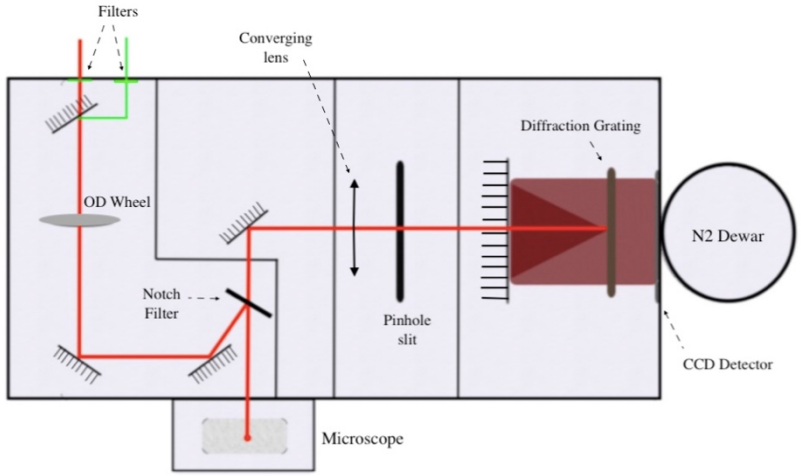

Figure 2.5: *A schematic of the inside of a Raman spectrometer. Adapted from [35]*

Many components in a LabRAM Raman spectrometer have already been described. In addition to these, mirrors are utilized to control the direction of the laser beam as well as converging lenses to focus the beam. The Nitrogen tank cools the CCD detector, reducing analysis time. Raman spectroscopy provides fingerprint spectra for many molecules and is particularly useful in the rapid analysis of drugs, with an increasing presence in forensic laboratories. This fingerprint spectral ability lends Raman spectroscopy to capabilities as a qualitative method. Quantitative analysis is also possible as concentration is a function of Raman peak intensity.

Chapter 3: Computational Chemistry

3.1. Introduction

Computational chemistry is a rapidly growing branch of chemical research that uses computational models to solve problems and simulate interactions. It is useful as a precursor to experimental work because computational chemistry can optimize molecular structures as well as simulate spectroscopic methods such as Raman or Infrared. Computational chemistry has also proven extremely valuable for the comparison of experimental results to theoretical data sets. All computational chemistry models aim to solve the Schrödinger Equation. Unfortunately, the Schrödinger Equation can only be solved exactly for a one electron system such as a hydrogen atom or He^+. If more than one electron is present, the Schrödinger Equation cannot be exactly solved due to Columbic interactions between electrons. Therefore, all computational chemistry models use complex theories to estimate a solution to the Schrödinger Equation, provided in **Equation 3.1**.

$$\hat{H}\Psi = E\Psi \qquad \textbf{(Equation 3.1)}$$

$\hat{H}$ represents the Hamiltonian operator, which is a sum of all the potential and kinetic energies of a system, and E represents the total energy of the system, or the Energy Eigenvalue. Therefore, the Schrödinger Equation is similar to the Law of Conservation of Energy in that the energy of a one electron system is completely conserved. Ψ represents the system's wave function, dependent upon the nucleus as well as electrons in the system. Many assumptions must be made so computational chemistry can successfully estimate solutions for large atoms and molecules. One of the first widely used computational

chemistry models was the Hartree-Fock (HF) method, which is dependent upon the Born-Oppenheimer approximation. This approximation assumes that the motion of an atom's nucleus is so slow relative to its electrons that it can be considered stationary. The Hartree-Fock method, also referred to as Self Consistent Field theory (SCF), treats each electron in a system as a singular orbital, independent of other electronic motion [36]. Hartree-Fock method designs a single Slater determinant based upon each electronic orbital. The HF method ignores Coulombic repulsion between electrons, resulting in severe underestimation of bond energies. Additionally, the wave function becomes overly complex with a large number of electrons, limiting the molecular size that Hartree-Fock was able to successfully compute. For this reason, Density Functional Theory (DFT) was introduced in 1964 and is now the most widely used method for computational quantum chemistry. DFT works around the complex multi-body wave function that Hartree-Fock is dependent upon and rather produces a single functional based upon the total electron density of a molecule [37].

$$\hat{H}(\rho) \approx \left[\hat{T} + \hat{V} + \hat{J} + \hat{E}\right](\rho) = \mathrm{E}(\rho) \quad \textbf{(Equation 3.2)}$$

Density Functional Theory suggests that all properties of a system, including electron correlation energies can be described using the total electron density. Therefore, the DFT functional is a function of electron density, which is in turn a function of the x, y and z position of individual electrons. This results in an ability to analyze larger molecules than previously with HF, as the parameters of the function depend on only three parameters, rather than 3N orbitals [38]. **Equation 3.2** provides the functions that the DFT functional is dependent upon to create an estimation for the Hamiltonian equation. In this, the energy eigenvalue is dependent upon the kinetic energy of the system (T), the potential

energy produced by electron interactions with the nucleus (V), electron repulsion energies (J), and the electron exchange energies (E) [39]. Additionally, the ρ symbol represents total electron density, indicating that the individual functionals are in fact functions of the total electron density of the system.

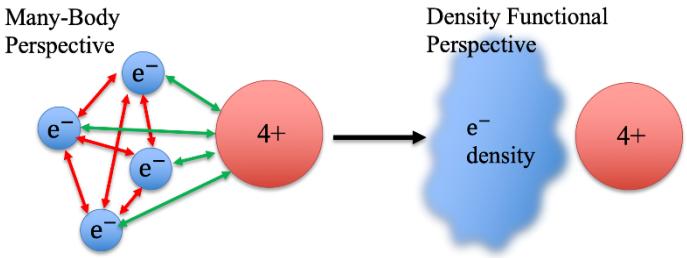

Figure 3.1: *Actual atomic interactions converted to the DFT perspective. Adapted from [40]*

3.2. Methods and Basis Sets

B3LYP is the most commonly used DFT hybrid functional method and represents "Becke 3-Parameter, Lee, Yang, Parr" which was named after the functional's creators. B3LYP combines theories behind both DFT and HF by attempting to estimate both exchange correlations as well as the dynamic electron correlations of a system. This accounts for Coulombic interactions between electrons as well as interactions between electrons and the nucleus. B3LYP/6-31g* is the method and basis set referred to as the industry standard and is particularly useful for organic molecules, but loses accuracy in the presence of metals [38]. Basis sets approximate atomic orbitals for the electrons in a given molecule which can be utilized by the computer to produce molecular orbitals and the subsequent wavefunction. In order to do this, the computer employs the Linear Combination of Atomic Orbitals (LCAO) approximation. The choice in basis set is a balance between computational cost and accuracy. The diffuse basis set used here, 6-311++G*(d,p),* is generally accepted as a sufficient final basis set for energy values, but is relatively a computationally expensive basis set.

Chapter 4: Previous Research

4.1. Previous Publications

Many studies have employed SERS (Surfaced Enhanced Raman Spectroscopy) in the analysis of Delta-9-Tetrahydrocannabinol and Cannabidiol, most with the objective to identify trace levels of cannabinoids in various mediums or surfaces. A 2016 SERS study detected trace amounts of Delta-9-THC deposited on silver nanoparticles and applied Density Functional Theory to characterize SERS modes of Delta-9-THC with the basis set 6-31G*(d,p)* [41]. The group also obtained a SERS spectrum for Delta-9-THC solvated in methanol, finding little difference in the Raman spectrum of Delta-9-THC solvated in methanol in the range of 400-1800 wavenumbers. Another study employed SERS to quantify trace levels of Delta-9-THC in body fluids and were able to identify characteristic C=C stretching modes of Delta-9-THC at 1603, 1556 and 1580 wavenumbers [42]. Moreover, an additional SERS study was able to characterize many Raman peaks for Delta-9-THC and identified a C-H stretching peak at 1605 wavenumbers as the most prominent peak even in the presence of complex biofluids [43]. Characteristic vibrational modes identified from previous works were useful in this study for identifying vibrational modes and their resulting shifts in the presence of solvents.

Despite vast research performed with SERS, very few studies have been performed on Cannabis and cannabinoids with Raman spectroscopy. One study obtained seized illicit drugs including Cannabis and analyzed each with various Raman spectrometers. The spectra obtained from each spectrometer ranged in quality, but none contained significant identifying spectral features [44]. Additionally, this study primarily applied Near-Infrared

excitation, likely the reason behind a lack of characteristic features being produced due to the low energy excitation. Another study used Raman microscopy to identify characteristic peaks of Delta-9-THCA, a precursor molecule to Delta-9-THC found in Cannabis plants [45]. A 2014 study by the Las Vegas Metropolitan Police Department produced a spectral library of illicit drugs through use of a portable Raman spectrometer. Therefore, in their analysis of Cannabis by Raman spectroscopy, Larkin's group published a reference spectrum of both Delta-9-THC and CBD, as provided in **Figure 4.1** [46]. The goal of this study was to produce the higher resolution Raman spectrum for Delta-9-THC and CBD ever reported, but the spectra produced by Larkin provided a reference for the accuracy of our results. Despite this, the spectrum obtained by the LVMPD did not include the vibrational modes such as O-H stretching occurring around 3800 cm^{-1}. These vibrational modes are important for the analysis of hydrogen bonding activity of the cannabinoids and therefore makes this work relevant in obtaining a full spectrum for both

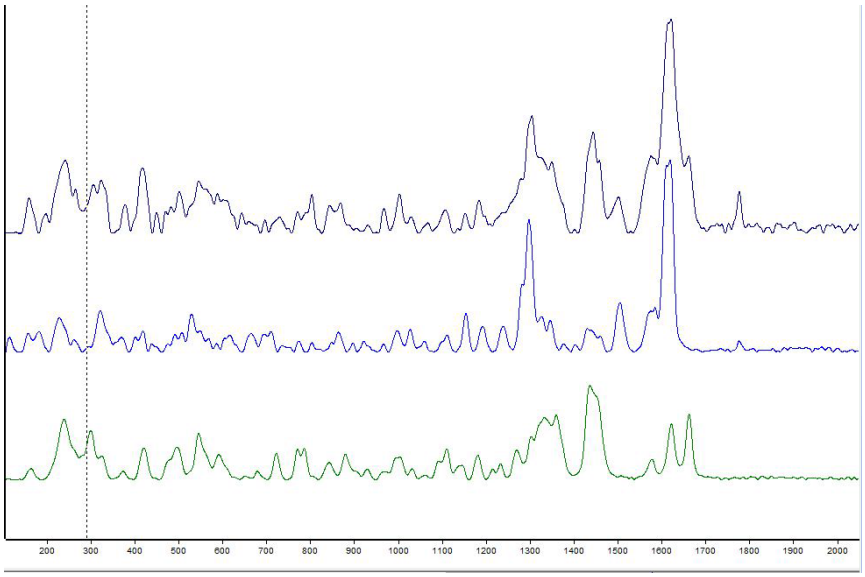

Figure 4.1: *Raman Spectra of Cannabis and cannabinoids obtained by LVMPD. Cannabis in black, Cannabidiol reference in blue, Delta-9-THC reference in green. Taken from [46]*

cannabinoids which includes this vibrational motion. The spectra in **Figure 4.1** was obtained using a portable Raman spectrometer equipped with a 785 nm laser.

Finally, significant Infrared spectra of both Delta-9-THC and Cannabidiol exist as spectra libraries [47],[48],[49]. A study published in 2020 analyzed the hydrogen bonding interactions between THC and Vitamin E Acetate (VEA) in both vaped and unvaped e-cigarette fluid [50]. This was done due to concern of VEA being potentially associated with lung injury when consumed in e-cigarettes or vaping devices. The study found that the O-H stretch of Delta-9-THC shifted to higher wavenumbers, a likely result of hydrogen bonding complexes being formed between Delta-9-THC and Vitamin E Acetate. Additionally, C-O stretching regions were identified in the complexes that were not in the reference spectra, located at 1736 and 1228 wavenumbers. IR has proven useful forensically for Cannabis identification, yet a significant drawback of Infrared spectroscopy exists especially for aqueous studies. This is the significant IR activity of water, which disrupts the IR spectra and hides vibrational modes. Water is significantly less Raman active, allowing Raman to succeed better in solvation studies. Despite this, IR vibrational frequencies are similar to those of Raman, allowing for further confirmation in the results of experimental spectra in this study.

4.2. Purpose of Study

The purpose of this study was to produce the highest resolution spectra ever reported for Δ^9-THC and Cannabidiol using Raman spectroscopy. By acquiring the highest resolution to date Raman spectrum for these cannabinoids, future work could be performed by use of Raman spectrometers for forensic applications or quality assurance purposes for analysis of commercial Cannabis products. This is important because as cannabinoids

become more openly accepted, consumer demand will only increase. Proper regulation and monitoring of Cannabis products begin with understanding chemical properties of the cannabinoids present.

Many studies have been performed to date using SERS analysis on cannabinoids, but Raman spectroscopy possesses advantages over SERS. Raman requires much less sample preparation, allowing for "point and shoot" analysis, resulting in reduced analysis time which in turn conserves resources. SERS also produces extreme amplification of signal, which may provide unrealistic results compared to field analysis. In contrast, Raman spectroscopy does not significantly manipulate the intensity produced by the sample of interest. This study seeks to expand Raman spectra of both Cannabidiol and Delta-9-THC that can be used for reference in future work as well.

Cannabinoids enter the blood stream and are likely to interact with solvents that may appear in the human blood stream. Additionally, cannabinoids interact with solvents in aforementioned Cannabis products. For these reasons, analysis of the interactions of Delta-9-THC and CBD with water and other solvents by Raman spectroscopy is a valid interest. Interactions between cannabinoid and solvent may influence energies or molecular conformation, potentially altering receptor interactions of Delta-9-THC and Cannabidiol. Shifts in the Raman spectrum relate to a change in the energy of a particular vibrational mode, which may be excited or relaxed by the presence of solvent molecules through noncovalent interactions. For example, vibrational modes may be relaxed by hydrogen bonding interactions that lower the energy of a polar bond in the molecule. For this reason, both Delta-9-THC and Cannabidiol were computationally analyzed in water, ethanol and methanol.

Chapter 5: Methodology

5.1. Experimental Methodology

5.1.1. Instrumentation

The instrument utilized in this study was a Horiba LabRAM HR Evolution Raman Spectrometer. The monochromatic light source was a Nd-YAG 532 nm laser, the highest energy laser equipped to this Raman spectrometer. Additionally, the detector was a CCD camera and the 10x microscope objective was used for every data acquisition. The instrument is usually equipped with a 600 gr/mm (grooves per millimeter) grating, but the 1800 gr/mm grating was primarily used in this study in an effort to acquire the highest possible resolution spectra possible.

Figure 5.1: *Horiba LabRAM HR Evolution Raman spectrometer. Taken from [51]*

5.1.1.1.Calibration

Before any Raman spectrum of the sample was acquired, a calibration of the spectrometer was performed using a silicone sample on a microscope slide. This was done to ensure that the Raman spectrometer was working correctly and obtaining consistent spectra in day to day operations. In order for this calibration to be successful, the silicon

peak produced using each laser was required to be within +/- 1 wavenumber of 520 cm^{-1} [52]. If this peak did not occur or was outside the accepted range, the instrument was not performing properly and data acquisition did not take place until the problem was solved.

5.1.1.2.Solid Phase

Crystalline Cannabidiol was graciously lent to the Hammer Research Group from the University of Mississippi Department of BioMolecular Sciences and all samples are to be returned upon a return to normalcy at the University of Mississippi. All Cannabidiol data acquisition was observed in the crystalline state. Additionally, analysis of crystalline Delta-9-THC was intended but was made impossible by the COVID-19 Pandemic, inhibiting further experimental research.

5.1.1.3.Solvation Studies

Because of the COVID-19 Pandemic, no experimental solvation studies could be performed and there was no procedure for solvated samples. Future work will involve the full solvation of Delta-9-THC and Cannabidiol in solvents, with analysis utilizing the cuvette attachment for the Raman spectrometer. Additionally, a custom-made vacuum chamber used by a previous member of the Hammer Research Group could be used for micro solvation of solvents in the presence of solid phase sample. Micro solvation allows for analysis with Raman active solvents without significant spectral interference.

5.2. Computational Methodology

5.2.1. Methods and Basis Sets

In order to perform the computations necessary for this study, Gaussian 09 and 16 programs were used. Additionally, programs such as Spectrum Simulator, Molekel and

Igor were utilized to produce theoretical spectra and optimized structures for the cannabinoids. The method employed in this study was B3LYP and the largest basis set was 6-311++G*(d,p)*, which was applied to all final computations performed, both optimizations and frequencies. Throughout the computational work, structures of isolated molecules as well as networks of cannabinoids and solvents were often optimized prior to Raman simulations. The relative energy of the system was determined through optimization, allowing for determination of the most likely low energy conformation. Following optimization, the checkpoint file was carried over and used for determination of the Raman vibrational frequencies. All computational Raman spectra were scaled by a correction factor of 0.97 to account for anharmonicity [53].

Chapter 6: Computational Results

6.1. Data Acquisition

The work included in this chapter employed computational chemistry to analyze hydrogen bonding activity for Delta-9-THC and Cannabidiol with water, ethanol and methanol. This analysis was performed by identifying how these interactions changed the cannabinoids' simulated energies and Raman spectra. To do this, computational Raman methods were applied to simulate Raman vibrational frequencies for both Delta-9-THC and Cannabidiol. In **Chapter 7**, the computational results are compared to experimental results to evaluate agreement between the two.

6.2. Delta-9-THC

6.2.1. Delta-9-THC Molecule

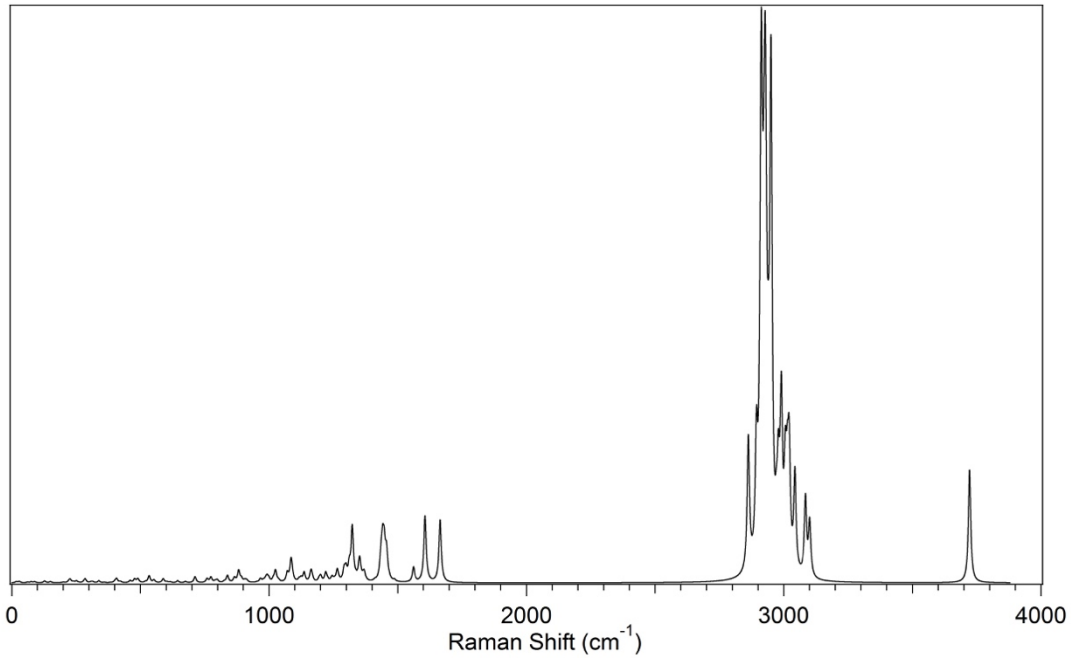

Figure 6.1: *Theoretical Raman spectrum of Delta-9-THC*

In order to identify the vibrational motions responsible for Raman peaks in the simulated spectra, the computational Raman spectra for each cannabinoid were analyzed utilizing the program GaussView. This program produced a simulated spectrum from the calculated Raman frequencies and was able to estimate the vibrational motion that produced each Raman peak. Additionally, chosen peaks were compared to previous publications that provided characteristic frequencies in order to confirm the accuracy of the GaussView program. **Table 6.1** provides characteristic frequencies chosen for Delta-9-Tetrahydrocannabinol. These frequencies are present in the simulated spectra in **Figure 6.1** and some of these peaks will allow for identification of Raman shifts by solvent presence in the next chapter.

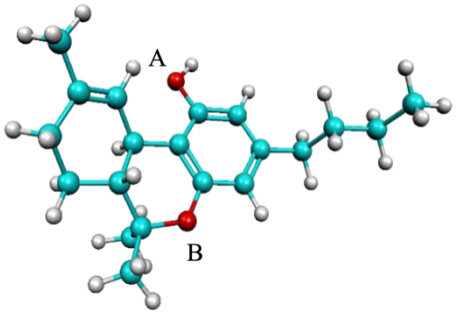

Vibrational Motion	Raman Shifts (cm^{-1})
Benzene Breathing/ C-C Stretch	1561.0, 1606.4
C=C Stretch	1664.6
C-H Deformations	1441.0, 3042.8
O-H Stretch	3721.1
Energy of Δ^9-THC	-5.834· 10^5 kcal/mol

Table 6.1: *Characteristic Raman frequencies of Delta-9-THC obtained computationally. Optimized Delta-9-THC structure included on the left.*

The relative energy of the system was obtained through optimization in the Gaussian program using DFT methods and is provided at the bottom of **Table 6.1**. To the left of the table is the expected lowest energy conformation for Delta-9-THC, obtained computationally and in agreement with the conformation observed in a previous DFT study with the same method and basis set [54]. Despite agreement in molecular orientation, the Borges study claimed no intramolecular hydrogen bond present in the Delta-9-THC

molecule due to electrostatic repulsion, yet this study found there to be a constant hydrogen bond occurrence between the phenol moiety and a terminal alkane off the methylcyclohexene ring. The potential reasons for this difference are unknown, especially since both this study and the Borges study utilized the same method and basis set. Solving this discontinuity could likely be done by optimizing Delta-9-THC under a different, but accurate, method and basis set to determine if this method suggested the presence of an internal hydrogen bond. The relative energy value for each conformation was obtained in Hartrees but was converted to units of kcal/mol, using a conversion factor of 1 Hartree = 627.5 kcal/mol. This energy value for the Delta-9-THC monomer will be compared to solvated computational results to propose the most stable hydrogen bonding positions for the three solvents.

6.2.2. Solvated Delta-9-THC

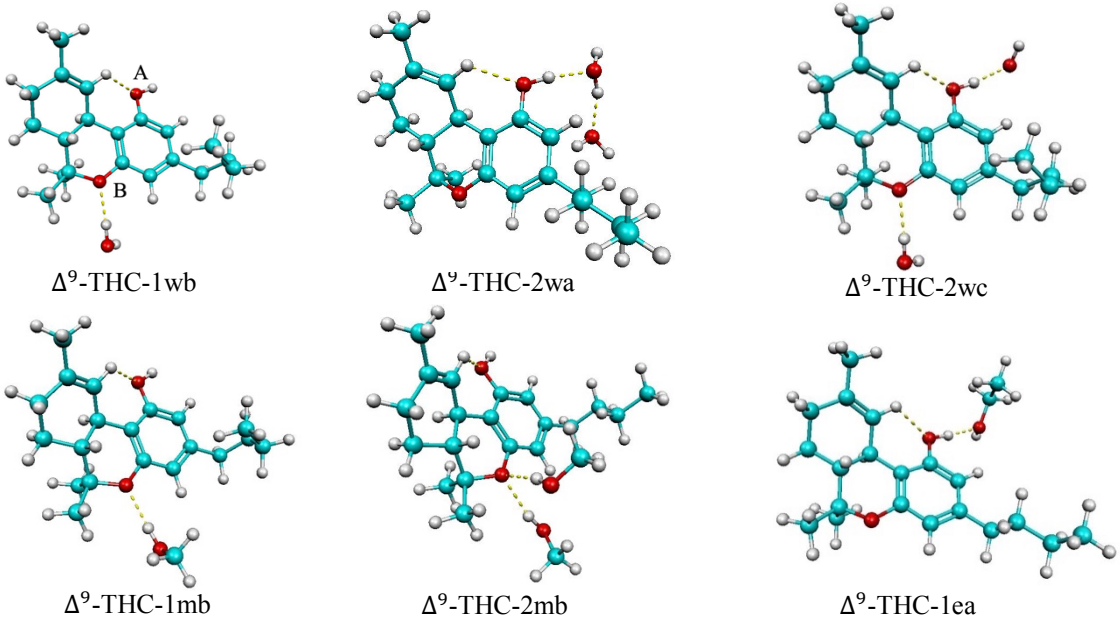

Figure 6.2: *Optimized molecular structures of* Δ^9*-THC in the presence of water, methanol and ethanol molecule(s)*

In order to better understand hydrogen bonding interactions of Delta-9-THC, computational chemistry was utilized to optimize molecular structures and produce simulated Raman spectra of Delta-9-THC with various solvent molecules. The solvent molecules were placed at different locations relative to the cannabinoid in order to determine the optimal hydrogen bonding location in the presence of each solvent. These results were compared and the lowest energy conformation was estimated based on the orientation with the lowest relative energy. Examples of optimized structures of Delta-9-THC in the presence of solvents are provided in **Figure 6.2**, with each structure labeled according to a labeling system described as follows. The number indicates the number of solvent molecules present, followed by a letter representing the solvent and finally A, B or C represents the location on the Delta-9-THC molecule where the solvent is hydrogen bonding. The C represents hydrogen bonding with both A and B locations, as Delta-9-THC possesses two hydrogen-bond acceptors, with one of these that also behaves as a hydrogen bond donator. Noticeably, some of the Delta-9-THC structures experience inward rotation of the alkyl chain, such as the 1wb and 1mb structures. Interestingly, as shown in the following table, these structures with an alkyl rotation also possess the least stable orientations based on relative energy values. For this reason, I hypothesize that it is unlikely for the alkyl chain to rotate inwards in a real hydrogen bonding system, as opposed to the theoretical models.

Computational System	Relative Energy (kcal/mol)
Δ^9-THC-1wa	0.0
Δ^9-THC-1wb	0.0
Δ^9-THC-2wa	0.48
Δ^9-THC-2wb	0.48
Δ^9-THC-2wc	0.0
Δ^9-THC-1ma	0.0
Δ^9-THC-1mb	0.0

Table 6.2: *Relative energy values for computational results of Delta-9-THC in the presence of various solvents.*

Table 6.2 provides relative energy values for the various systems containing solvents and Delta-9-THC, with the most negative energy value of the lowest energy Delta-9-THC system for each type established as zero, which is in turn the most probable stable orientation. Other values that are not zero represent a difference in energy of each system as compared to the zero value for that system. The relative energy values suggest that for the Delta-9-THC 2w structures, the A and B positions are equivalent in energy, but when both positions are occupied with hydrogen bonding during the same calculation, as in the 2wc structure, the relative energy becomes significantly more negative. This suggests that the 2wc structure is more stable than both the 2wa and 2wb structures. The A and B positions are equivalent in energy for methanol, suggesting in the presence of one methanol, the A and B positions are equally likely to hydrogen bond. Future work will include the analysis of large hydrogen-bonding networks with the cannabinoids and solvents, to better understand the preferences of the cannabinoids for hydrogen bonding.

Figure 6.3 includes the Raman spectra of Delta-9-THC as water molecules are introduced, interacting at various locations on the molecule. The corresponding label for each Raman spectra is written alongside, signifying the point of interaction and number of water molecules present. The greatest difference across the spectra is observed in the O-H stretch of Delta-9-THC, occurring at 3721.1 cm^{-1} for the monomer. The introduction of water molecules subsequently induces a red shift, or a shift to shorter wavenumbers, in the Delta-9-THC O-H stretch by usually no more than thirty wavenumbers. The greatest agreement with the monomeric Raman spectra occurs with the 1wb structure, especially obvious due to the presence of a C-H deformation peak at 3042 wavenumbers in the CBD spectrum. The 1wb spectrum is the only CBD-water spectrum in which this peak exists or is resolved enough to be identified.

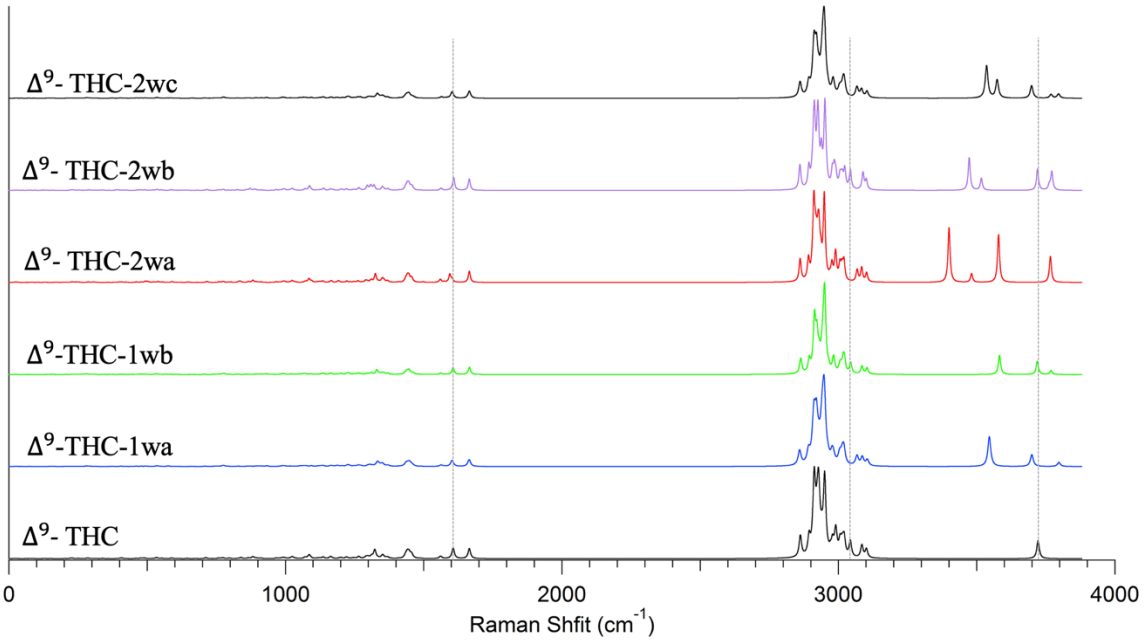

Figure 6.3: *Theoretical Raman spectra of Delta-9-THC with addition of water molecules at different locations on the cannabinoid*

In order to determine the degree of vibrational shifting as a result of solvent introduction, the initial characteristic frequencies of the Delta-9-THC monomer were compared to the observed vibrational frequencies from computational solvation studies.

These frequencies are provided in **Table 6.3**, in which interesting information was acquired. We were ultimately able to conclude that the A position of Delta-9-THC contributed the most variation to theoretical Raman spectra when participating in hydrogen bonding with a solvent. Hydrogen bonding at the B position induced significantly less variation in the O-H stretching frequency compared to the Delta-9-THC monomer.

Vibrational Motion	Raman Shift (cm^{-1}) Δ^9-THC	RS 1wa	RS 1wb	RS 2wa	RS 2wb	RS 2wc	RS 1ma	RS 1mb	RS 1ea
Benzene Breathing/ C-C Stretch	1561.0, 1606.4	1560.7, 1602.8	1559.0, 1605.8	1560.0, 1594.4	1563.2, 1608.6	1563.9, 1602.8	1563.8, 1602.8	1561.9, 1607.0	1536.8, 1602.9
C=C Stretch	1664.6	1663.9	1665.0	1664.9	1664.7	1664.6	1664.4	1664.8	1664.6
C-H Deformation	1441.0, 3042.8	1445.8, ----	1442.9, 3044.0	1442.6, ----	1443.4, 3042.5	1443,3, ----	1443.4, ----	1446.9, ----	1441.9, ----
O-H Stretch	3721.72	3697.3	3719.4	3766.3	3719.8	3697.6	3727.8	3719.5	3720.2

Table 6.3: *Characteristic Raman frequencies of Delta-9-THC and resulting shifts in the presence of solvent molecule(s)*

This trend in hydrogen bonding positions is potentially a result of the B position behaving solely as a hydrogen acceptor, whereas the A position can both donate its hydrogen and accept hydrogens from other atoms. Furthermore, the greatest variation in theoretical Raman spectra for all vibrations occurred between the 2wa complex and the Delta-9-THC monomer. The C=C stretch occurring at 1664.6 cm^{-1} for the Delta-9-THC monomer did not experience shifts greater than one wavenumber by any solvent interactions, suggesting it is not affected by the presence of hydrogen-bonding solvents. Nevertheless, identification of characteristic frequencies for Delta-9-THC is important to further the capabilities of Raman as method for analysis of cannabinoids. An interesting occurrence was at 3042.8 cm^{-1} for the Delta-9-THC monomer, likely a C-H deformation. In all water conformations besides 1wb, this peak was not present in theoretical spectra. It

was in fact present in the 1wb spectrum and within 2 wavenumbers of the monomeric spectrum. This further supports the argument that Delta-9-THC experiences the least spectral variation in the presence of water if the B position is hydrogen bonding.

6.3. Cannabidiol

6.3.1. Cannabidiol Molecule

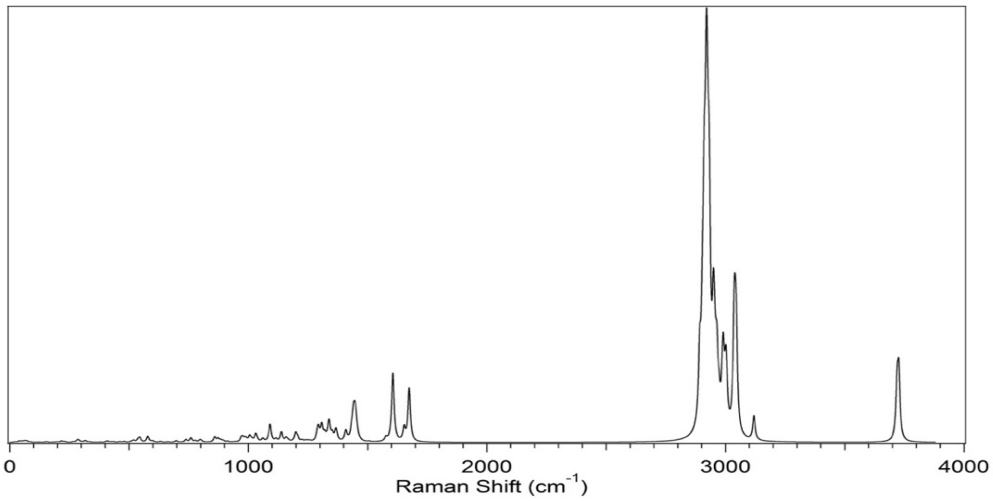

Figure 6.4: *Theoretical Raman spectrum of Cannabidiol*

Cannabidiol was especially difficult to optimize due to the terminal alkene in close proximity to a phenol. Many optimizations either failed or resulted in the removal of a phenol group from the Cannabidiol to become a free water molecule, resulting in a loss of the terminal alkene as well. The final optimization resulted in strong repulsion between the terpene ring and both phenols of CBD, as was confirmed in the Borges study. The theoretical Raman spectra for a single molecule of Cannabidiol is provided in **Figure 6.4**. As elucidated in **Chapter 7**, there is significant agreement between experiment and theory for this molecule. **Table 6.4** provides characteristic vibrational frequencies of Cannabidiol as well as the relative energy of the monomer, alongside an optimized structure of Cannabidiol. Potential hydrogen bonding positions for Cannabidiol are labeled on this

optimized structure provided. These are designated as A or B and were applied to the naming system used for the optimized structures. Fewer sources were available for the characterization of CBD vibrational modes, but most modes chosen were in close agreement to the characterized modes determined for Delta-9-THC and GaussView was also applied to predict these modes.

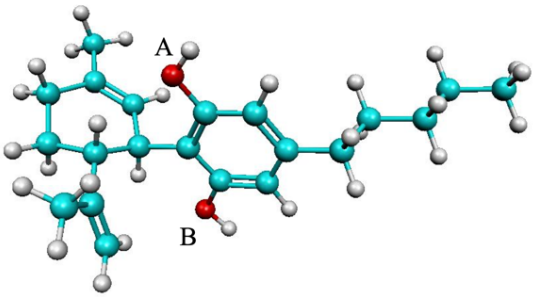

Vibrational Motion	Raman Shifts (cm^{-1})
Benzene Breathing/ C-C Stretch	1605.8
C=C Stretch (ring)	1674.2
C=C Stretch (alkene)	1653.1
O-H Stretch	3719.4, 3724.5
C-H Deformation	2921.2, 3038.5, ----, 3119.4
Energy of CBD	$-6.081 \cdot 10^5$ kcal/mol

Table 6.4: *Characteristic Raman frequencies of CBD obtained computationally. Optimized Cannabidiol structure included on the left.*

6.3.2. Solvated Cannabidiol

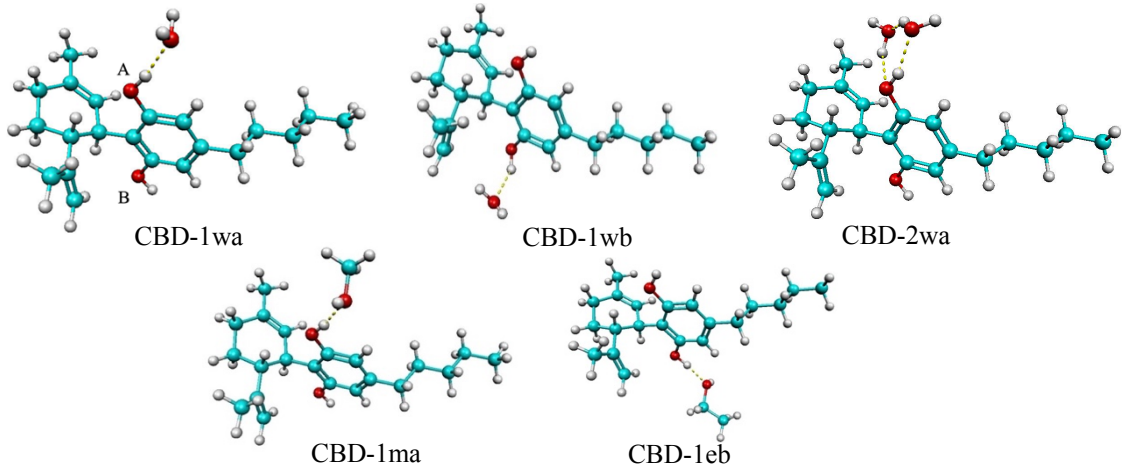

Figure 6.5: *Optimized molecular structures of Cannabidiol in the presence of water, methanol and ethanol molecule(s)*

Water, ethanol and methanol were chosen again for theoretical analysis of solvated Cannabidiol for the same reasons mentioned previously in **Chapter 1.3.3**. Cannabidiol is arguably consumed by a greater proportion of the population as its use is allowed in many states where Cannabis is illegal. Therefore, its potential for interaction with solvents may be even greater than that of Delta-9-THC. The same labeling system was utilized for Cannabidiol as was for Delta-9-THC. Due to the difficulties in optimizing the molecular structure of the Cannabidiol monomer, fewer solvated CBD structures were obtained when compared to Delta-9-THC, but at least one structure representative of each solvent was calculated, are provided in **Figure 6.5**. Additionally, Cannabidiol possesses two phenol groups whereas Delta-9-THC possesses one phenol and a furan ring structure. Therefore, it was hypothesized that the A and B positions of Cannabidiol would produce identical

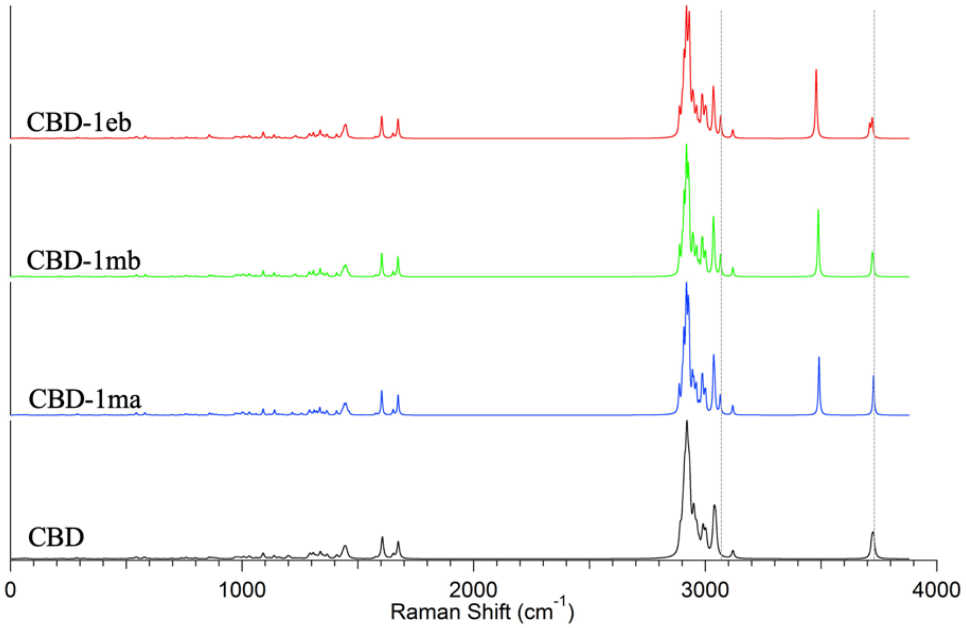

Figure 6.6: *Theoretical Raman Spectra for CBD Monomer, CBD-1ma, CBD-1mb and CBD-1eb. Naming System defined in text.*

results. Nevertheless, both A and B positions were obtained for as many solvents as possible, limited only by the significant computer time and cost required by each computation due to the size of the cannabinoid.

Figure 6.6 provides a comparison of the theoretical Raman spectra of the Cannabidiol monomer along with the 1ma, 1mb and 1eb structures. This is in contrast to **Figure 6.3** to the Delta-9-THC section, which compared Raman shifts for water. This figure represents Cannabidiol and the subsequent Raman spectra for CBD interacting with methanol and ethanol molecules. Generally, shifts to the O-H stretching frequency at 3725 wavenumbers were minimal for Cannabidiol as compared to Delta-9-THC results, but the most significant difference being present in the 1eb structure. The two phenol groups of CBD split frequencies in the 1eb structure, with one peak at 3720.8 and the other at 3710.2 wavenumbers. Therefore, red shifts of ten and six wavenumbers occurred as a result of one phenol group interacting with a molecule of ethanol. Additionally, a peak at located around 3063-3065 wavenumbers is present in each solvated theoretical spectrum for Cannabidiol but is not present in the spectrum of the monomer. It is possible the monomeric peak at 3040 wavenumbers covers this peak and it isn't until a solvent is introduced that the peak shifts and allows for resolution of both peaks. Further comparison of Raman shifts due to solvent interactions are provided in **Table 6.6.**

Computational System	ΔE (kcal/mol)
CBD-1wa	0.0
CBD-1wb	0.0
CBD-1ma	0.0
CBD-1mb	0.0

Table 6.5: *Relative energy values for computational results of CBD in the presence of various solvents.*

Similar to the work performed for Delta-9-THC, the relative energy values for Cannabidiol were determined through computational optimization. This data is provided in **Table 6.5**, including the relative energies for hydrogen-bonding locations with water and methanol, resulting in estimations of lowest energy conformations for CBD with solvents. Relative energies suggest no preference to the A or B positions, consistent with the fact that the two phenol groups are virtually identical. Therefore, further theoretical work will likely ignore the comparison of favorable hydrogen bonding locations on CBD, as it would be difficult to predict which of the two seemingly equivalent phenol groups would interact through hydrogen bonding with a solvent. This is different from Delta-9-THC because Delta-9-THC has two oxygen molecules that are not necessarily equivalent, as one can behave as a hydrogen bond donor and the other cannot.

Table 6.6 provides characteristic frequencies for the Cannabidiol monomer along with corresponding computational Raman shifts for CBD with solvent molecules. These characteristic frequencies were chosen based upon identified frequencies for Delta-9-THC as well as their significance as the most intense peaks identified from the CBD monomeric spectrum. The most significant difference in overall Raman spectra between monomer and solvated CBD occurred in the 1wb structure, as can be concluded by the differences for the

C-C stretch and the fourth C-H deformation. This is particularly interesting because for Delta-9-THC, this structure possessed the least variation in Raman shifts. Additionally, it appears that significant variation of O-H Raman shifts in CBD do not occur due to hydrogen bonding with solvents, with carbon stretching modes providing greater information about hydrogen bonding. This is different than the Delta-9-THC, in the O-H stretch commonly experienced the greatest variation due to solvent introduction. The bolded C-H deformation peaks in **Table 6.6** represent the most intense peak in all theoretical spectra, which does not significantly shift as a result of any solvent introduction.

Vibrational Motion	**Raman Shift (cm^{-1}) *CBD***	**RS 1wa**	**RS 1wb**	**RS 2wa**	**RS 1ma**	**RS 1mb**	**RS 1eb**
Benzene Breathing/ C-C Stretch	1605.8	1603.5	1600.2	1607.4	1603.0	1603.2	1603.0
C=C Stretch (ring)	1674.2	1673.9	1675.2	1666.3	1673.7	1673.1	1673.4
C=C Stretch (alkene)	1653.1	1652.3	1641.0	1663.4	1652.3	1651.9	1651.7
O-H Stretch	3719.4, 3726.4	3726.6	3719.1	3725.9	3726.5	3721.1	3710.2, 3720.7
C-H Deformation	**2921.2**, 3038.5, ----, 3119.4	**2918.9**, 3036.3, 3063.7, 3118.4	**2919.5**, 3036.8, 3065.6, 3103.5	**2919.8**, 3037.9, 3036.6, 3118.1	**2919.1**, 3036.6, 3064.4, 3118.5	**2919.1**, 3035.0, 3065.7, 3118.8	**2919.1**, 3035.0, 3066.5, 3118.7

Table 6.6: *Characteristic Raman frequencies of CBD and resulting shifts in the presence of solvent molecule(s)*

Chapter 7: Experimental Results and Data Analysis

7.1. Delta-9-THC

Samples of Delta-9-THC were expected to be received following the University of Mississippi's Spring Break period. Due to the outbreak of COVID-19 and subsequent cancellation of University activities, further experimental data acquisition using the Raman spectrometer was impossible. Therefore, no experimental spectrum of Delta-9-THC was acquired in this study as was previously intended, nor was experimental spectrum acquired for solvated Delta-9-THC.

7.2. Cannabidiol

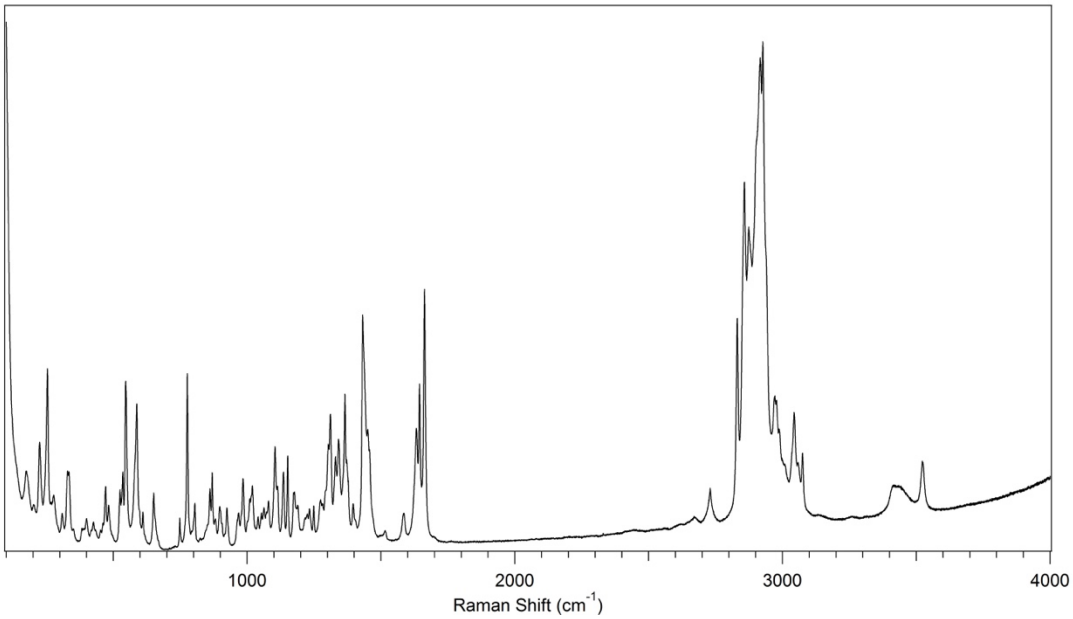

Figure 7.1: *Experimental Raman spectrum of Cannabidiol*

Successful Raman spectra of Cannabidiol was acquired, and this is provided in **Figure 7.1**. This was obtained using a 1800 grooves/mm grating and the instrument's Nd-YAG 532-nm laser. Additionally, there was no baseline correction and the acquisition time was 5 per minute while the accumulation time was 10 per minute. **Figure 7.1** provides a

high-resolution Raman spectrum of Cannabidiol that includes O-H stretching frequencies around 3700 wavenumbers which was not included in the reference Raman spectrum obtained by the Las Vegas Metropolitan Police Department, provided in **Figure 4.1**. We predicted this O-H stretching region most likely to be affected by the presence of hydrogen bonding solvents.

7.3. Comparison of Experiment to Theory

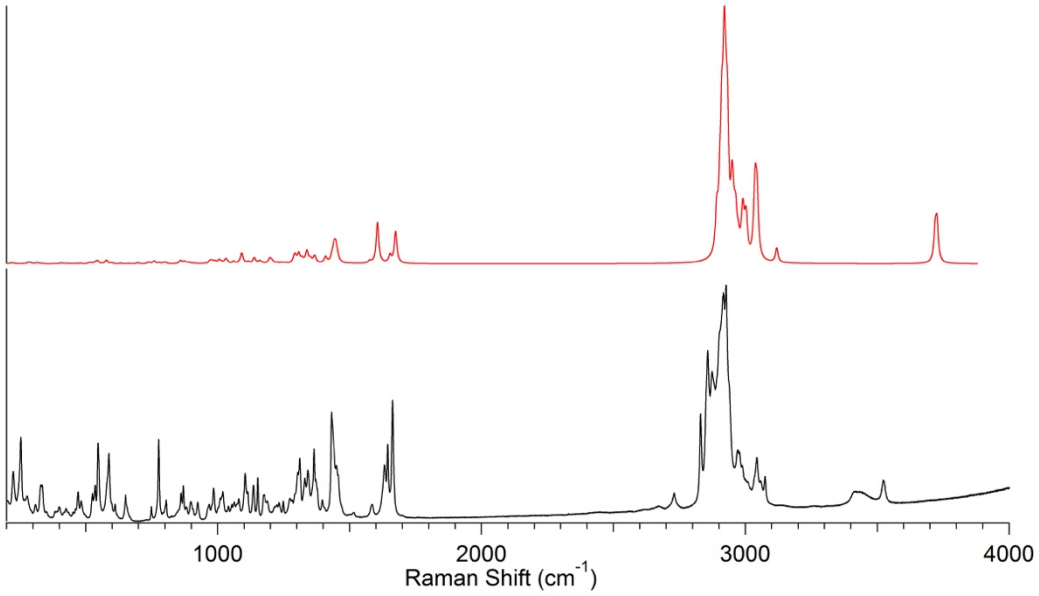

Figure 7.2: *Comparison of experimental Cannabidiol spectrum to theoretical spectrum. Theory is above in red and experiment is below in black.*

Through analysis of the theoretical Cannabidiol Raman spectrum, there is strong agreement between experiment and theory. An intense peak at 2921 cm^{-1} is shared between the two spectra, along with a less intense peak at 1674 cm^{-1}. Conversely, peaks are present in experimental results that are not observed in the theoretical spectrum. In addition to this, the low energy vibrational modes are significantly less intense in theory than in the experimental spectra. This difference in peak intensity may be attributed to greater concentration of the sample compared to a single theoretical molecule. It may also be a result of the intense incident light from the 532 nm laser, as a specific laser source is not

accounted for in theoretical calculations. The most dramatic peak difference occurs for the O-H stretching region, in which the experimental CBD spectrum experiences a shift to shorter wavenumbers with a difference of nearly two hundred wavenumbers. This dramatic red shift may likely be contributed to bonding stabilization between the individual CBD molecules that form the crystalline solid. Additionally, the broadened peak to the left of the O-H peak could be the second O-H peak of Cannabidiol, which had been hidden in theory by overlap of the two modes. The broadening of the peak may also be attributed to hydrogen bonding between individual Cannabidiol molecules, further signifying the need for further work to be done involving the computational and experimental solvation of cannabinoid networks in addition to the already analyzed monomers.

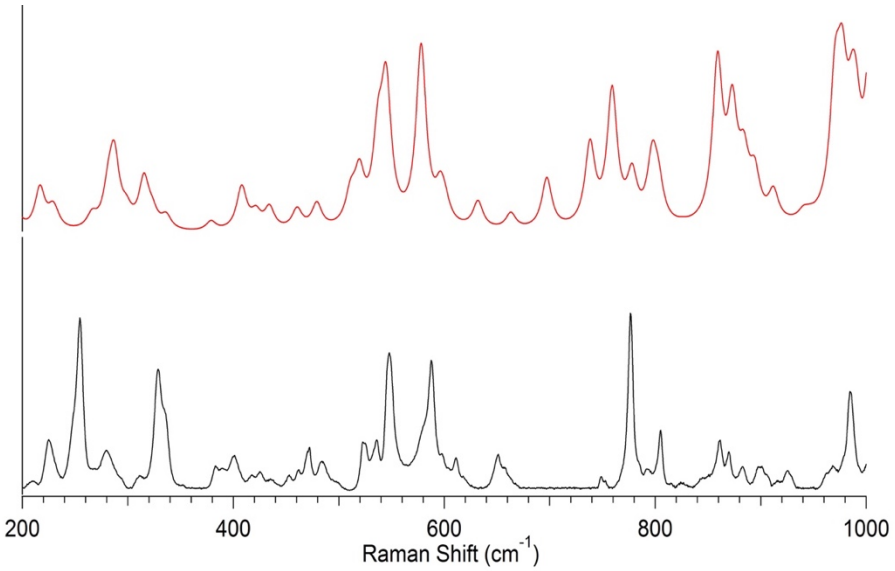

Figure 7.3: *Low frequency vibrational modes of Cannabidiol theory (red) and Cannabidiol experiment (black).*

The low frequency region shown in **Figure 7.3** displays strong agreement between experiment and theory, with significant overlap for peaks between 540-600 wavenumbers. There are peaks in the theory that are not present in the experimental spectrum, such as the peak at 710 wavenumbers. In general, there is significant agreement between experiment

and theory, suggesting the experimental results are acceptable at low frequency modes. Following this, the experimental spectrum for Cannabidiol was compared to the spectrum obtained by the Larkin group and the theoretical Cannabidiol spectrum that this group obtained. **Figure 7.4** compares all three of these spectra to determine the match-up between experiment and theory.

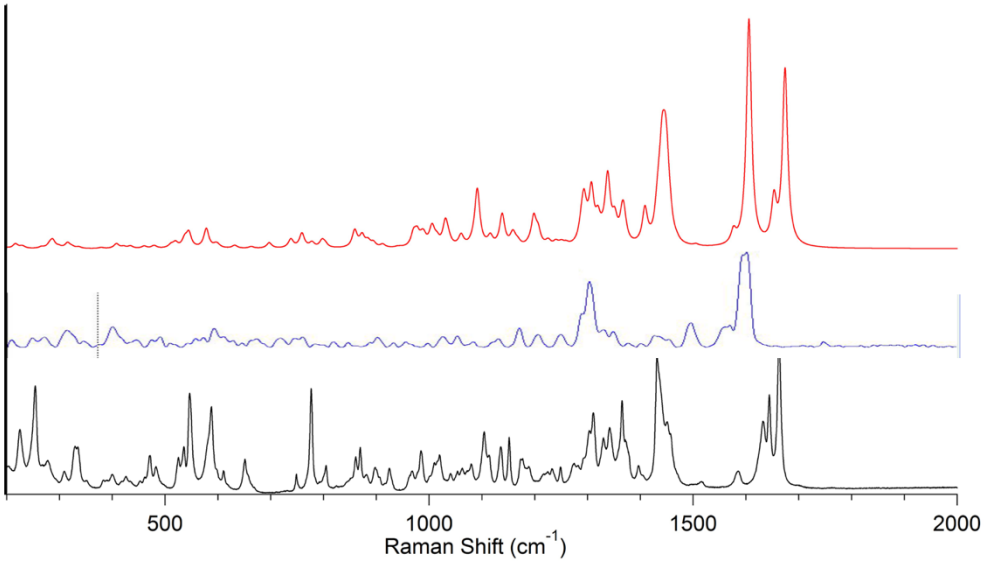

Figure 7.4: *Theoretical Raman for CBD in red, Larkin Group Raman spectrum of CBD in blue and our spectrum of CBD in black. Blue spectrum taken from [46]*

Analysis of **Figure 7.4** suggests that both the blue spectra and the black spectra possess peaks that agree with theory almost exactly. Despite this, some peaks in the Larkin spectrum are not present in this study's Raman spectrum of CBD, or are significantly less intense. An example of this is observed in the theoretical C-C stretch observed at 1605 wavenumbers that is significantly less intense in our spectrum as compared to theory and the Larkin spectrum. In contrast, peaks exist in this study's spectrum that agree with theory but are not present in the Larkin spectrum. Examples of this are the region around 500 wavenumbers, which is much more intense in our spectrum as well as the alkene stretch occurring at 1674 wavenumbers, which is slight red shifted in our spectrum but is not

present in the Larkin spectrum. The peaks obtained in this study are more easily identified in addition to being more intense. Because some peaks appear in each experimental spectrum that are not present in the other spectrum, yet both agree with theory, suggests that both are important to further identify Raman peaks for Cannabidiol. Despite this, I argue that this study has successfully produced a Raman spectrum for Cannabidiol that is of higher resolution than what has previously been published. Additionally, the Raman spectrum produced in this study also includes the O-H stretching region for Cannabidiol, which has shown to experience shifting due to hydrogen bonding interactions with solvents and with other monomeric units of CBD.

Chapter 8: Conclusions

The goal of this study was to obtain the highest resolution Raman spectra ever recorded for Delta-9-Tetrahydrocannabinol and Cannabidiol. Additionally, this study intended to review literature related to this study and utilize computational chemistry to assess the impact of hydrogen bonding on the cannabinoids' energies and theoretical Raman spectra, obtaining the expected lowest energy conformations in the process. The COVID-19 Pandemic caused experimental spectra to be limited, but a Raman spectrum of CBD was successfully obtained. The high-resolution Raman spectrum of CBD including both low frequency vibrational modes as well as a full spectrum reaching 4000 cm^{-1}, which had been excluded in a previous Raman spectroscopy study of Cannabis [46]. Moreover, successful results were obtained utilizing computational chemistry including hydrogen bonding interactions, as well as probable lowest energy conformations. Optimized structures suggested the alkane chain of Delta-9-THC sometimes rotates inward when solvents are present, while CBD does not exhibit this. Additionally, the structures in which the alkane chain has turned inward are also the structures where Delta-9-THC was least stable according to relative energy values. The theoretical Raman spectra for Delta-9-THC and CBD in the presence of water, ethanol and methanol in various conformations were analyzed to determine the impact of hydrogen bonding events on the Raman shifts observed. It was concluded that the A hydrogen-bonding position of Delta-9-THC contributed the most significant shifts to Raman frequencies, particularly the O-H stretch. In contrast, the A and B positions did not significantly differ in CBD theory.

Chapter 9: Future Work and Applications

Due to limitations created by the COVID-19 Pandemic, continuation of the original goals of this study will be included in future work, which would involve both solid state and solvated experimental spectra for comparison with computational spectra. These solvated studies could be performed with both the full solvation of cannabinoids as well as application of the Hammer Research Group's micro solvation chamber. Additionally, future computational work could include analysis of dimers and trimer crystal structures of the cannabinoids, as this likely has an impact on real hydrogen-bonding interactions. These computational structures were not included in the current study due to the tremendous computational cost. Because it is increasingly important to understand interactions between cannabinoids, future work could analyze interactions between Cannabidiol and Delta-9-THC. Treatment studies have shown that Cannabidiol may induce synergistic effects to Delta-9-THC so their interactions could be explained through application of Raman spectroscopy [21]. In addition to direct action between the two, other factors such as interactions with metabolizing enzymes in the ECS could play a role in synergistic properties. Analysis of cannabinoids in commercial products such as CBD oil could further Raman spectroscopy's potential to serve as a tool for both identification and quality assurance methods.

References

1. Pritchard, H.O. and H.A. Skinner, *The Concept Of Electronegativity.* Chemical Reviews, 1955. **55**(4): p. 745-786.
2. Ashish, *Is Carbon Dioxide (CO2) Polar or Nonpolar? Science*ABC, 2017.
3. Musto, D.F., *The Marihuana Tax Act of 1937.* Archives of General Psychiatry, 1972. **26**(2): p. 101-108.
4. Bauman, A. and P. Phongsavan, *Epidemiology of substance use in adolescence: prevalence, trends and policy implications.* Drug and Alcohol Dependence, 1999. **55**(3): p. 187-207.
5. Mead, A., *Legal and Regulatory Issues Governing Cannabis and Cannabis-Derived Products in the United States.* Frontiers in plant science, 2019. **10**: p. 697-697.
6. NCIA, *State-by-State Marijuana Policies.* The Cannabis Industry.
7. ElSohly, M. and W. Gul, *Constituents of cannabis sativa.* Handbook of cannabis, 2014. **3**: p. 1093.
8. Russell, C., et al., *Routes of administration for cannabis use – basic prevalence and related health outcomes: A scoping review and synthesis.* International Journal of Drug Policy, 2018. **52**: p. 87-96.
9. Bisogno, T., A. Ligresti, and V. Di Marzo, *The endocannabinoid signalling system: biochemical aspects.* Pharmacology Biochemistry and Behavior, 2005. **81**(2): p. 224-238.
10. Kalant, H., *Medicinal Use of Cannabis: History and Current Status.* Pain research & management : the journal of the Canadian Pain Society = journal de la société canadienne pour le traitement de la douleur, 2001. **6**: p. 80-91.
11. Gong, J.-P., et al., *Cannabinoid CB2 receptors: immunohistochemical localization in rat brain.* Brain research, 2006. **1071**(1): p. 10-23.
12. Pertwee, R.G., *The diverse CB1 and CB2 receptor pharmacology of three plant cannabinoids: Δ9-tetrahydrocannabinol, cannabidiol and Δ9-tetrahydrocannabivarin.* British Journal of Pharmacology, 2008. **153**(2): p. 199-215.
13. Zou, S. and U. Kumar, *Cannabinoid Receptors and the Endocannabinoid System: Signaling and Function in the Central Nervous System.* International journal of molecular sciences, 2018. **19**(3): p. 833.
14. Fernández-Ruiz, J., et al., *Cannabidiol for neurodegenerative disorders: important new clinical applications for this phytocannabinoid?* British journal of clinical pharmacology, 2013. **75**(2): p. 323-333.
15. Li, H., et al., *Overview of cannabidiol (CBD) and its analogues: Structures, biological activities, and neuroprotective mechanisms in epilepsy and Alzheimer's disease.* European Journal of Medicinal Chemistry, 2020. **192**: p. 112163.
16. Banister, S.D., et al., *Dark Classics in Chemical Neuroscience: Δ9-Tetrahydrocannabinol.* ACS Chemical Neuroscience, 2019. **10**(5): p. 2160-2175.
17. Elkins, A.C., et al., *Development of a validated method for the qualitative and quantitative analysis of cannabinoids in plant biomass and medicinal cannabis resin extracts obtained by super-critical fluid extraction.* Journal of Chromatography B, 2019. **1109**: p. 76-83.
18. Lovestead, T.M. and T.J. Bruno, *Determination of Cannabinoid Vapor Pressures to Aid in Vapor Phase Detection of Intoxication.* Forensic chemistry (Amsterdam, Netherlands), 2017. **5**: p. 79-85.

19. Pertwee, R.G., *Pharmacology of cannabinoid CB1 and CB2 receptors.* Pharmacology & Therapeutics, 1997. **74**(2): p. 129-180.
20. Noyes Jr, R., et al., *Analgesic effect of delta-9-tetrahydrocannabinol.* The Journal of Clinical Pharmacology, 1975. **15**(2-3): p. 139-143.
21. Whittle, B.A., G.W. Guy, and P. Robson, *Prospects for New Cannabis-Based Prescription Medicines.* Journal of Cannabis Therapeutics, 2001. **1**(3-4): p. 183-205.
22. Mechoulam, R., L.A. Parker, and R. Gallily, *Cannabidiol: an overview of some pharmacological aspects.* The Journal of Clinical Pharmacology, 2002. **42**(S1): p. 11S-19S.
23. Friedman, D. and J.I. Sirven, *Historical perspective on the medical use of cannabis for epilepsy: Ancient times to the 1980s.* Epilepsy & Behavior, 2017. **70**: p. 298-301.
24. Rock, E., et al., *Cannabidiol, a non-psychotropic component of cannabis, attenuates vomiting and nausea-like behaviour via indirect agonism of 5-HT1A somatodendritic autoreceptors in the dorsal raphe nucleus.* British Journal of Pharmacology, 2012. **165**(8): p. 2620-2634.
25. Lastres-Becker, I., et al., *Cannabinoids provide neuroprotection against 6-hydroxydopamine toxicity in vivo and in vitro: relevance to Parkinson's disease.* Neurobiology of disease, 2005. **19**(1-2): p. 96-107.
26. Russo, E. and G.W. Guy, *A tale of two cannabinoids: the therapeutic rationale for combining tetrahydrocannabinol and cannabidiol.* Medical hypotheses, 2006. **66**(2): p. 234-246.
27. Hazekamp, A., *The Trouble with CBD Oil.* Medical Cannabis and Cannabinoids, 2018. **1**(1): p. 65-72.
28. Lukas, S.E. and S. Orozco, *Ethanol increases plasma Δ9-tetrahydrocannabinol (THC) levels and subjective effects after marihuana smoking in human volunteers.* Drug and Alcohol Dependence, 2001. **64**(2): p. 143-149.
29. Doctorate, S.M., *Introduction to the Electromagnetic Spectrum.* National Aeronautics and Space Administration,, 2010.
30. Contributors, W., *Morse Potential.* Wikipedia, the Free Encyclopedia, 2020.
31. Ferraro, J.R., *Introductory raman spectroscopy*2003: Elsevier.
32. Bumbrah, G.S. and R.M. Sharma, *Raman spectroscopy – Basic principle, instrumentation and selected applications for the characterization of drugs of abuse.* Egyptian Journal of Forensic Sciences, 2016. **6**(3): p. 209-215.
33. Muoura, C.C., Rahul S. Tare, Rochard O. C. Oreffo, Sumeet Mahajan, *Raman Spectroscopy and coherent anti-Stokes Raman scattering imaging: prospective tools for monitoring skeletal cells and skeletal regeneration.* Journal of The Royal Society Interface 2016. **13**.
34. Mutsaers, M., *Zika vector control: Near infrared spectroscopy predicting Wolbachia infection in post-mortem Aedes aegypti*, 2018.
35. Artur, C.G., *Fundamental Investigations into Single Molecule Surface Enhanced Raman Spectroscopy.* 2014.
36. Sherrill, C.D., *An introduction to Hartree-Fock molecular orbital theory.* School of Chemistry and Biochemistry Georgia Institute of Technology, 2000.
37. Hasnip, P.J., et al., *Density functional theory in the solid state.* Philosophical Transactions of the Royal Society A: Mathematical, Physical and Engineering Sciences, 2014. **372**(2011): p. 20130270.
38. Orio, M., D.A. Pantazis, and F. Neese, *Density functional theory.* Photosynthesis research, 2009. **102**(2-3): p. 443-453.

39. Cohen, A.J., P. Mori-Sánchez, and W. Yang, *Challenges for density functional theory.* Chemical Reviews, 2012. **112**(1): p. 289-320.
40. Lusk, M. and A. Mattsson, *High-performance computing for materials design to advance energy science.* MRS Bulletin, 2011. **36**.
41. Yüksel, S., et al., *Trace detection of tetrahydrocannabinol (THC) with a SERS-based capillary platform prepared by the in situ microwave synthesis of AgNPs.* Analytica Chimica Acta, 2016. **939**: p. 93-100.
42. Sivashanmugan, K., et al., *Trace Detection of Tetrahydrocannabinol in Body Fluid via Surface-Enhanced Raman Scattering and Principal Component Analysis.* ACS Sensors, 2019. **4**(4): p. 1109-1117.
43. Sivashanmugan, K., Y. Zhao, and X.A. Wang, *Tetrahydrocannabinol Sensing in Complex Biofluid with Portable Raman Spectrometer Using Diatomaceous SERS Substrates.* Biosensors, 2019. **9**(4).
44. Hargreaves, M.D., et al., *Comparison of near infrared laser excitation wavelengths and its influence on the interrogation of seized drugs-of-abuse by Raman spectroscopy.* Journal of Raman Spectroscopy, 2009. **40**(12): p. 1974-1983.
45. Garbacik, E., et al., *In planta imaging of Δ9-tetrahydrocannabinolic acid in Cannabis sativa L. with hyperspectral coherent anti-Stokes Raman scattering microscopy.* Journal of Biomedical Optics, 2013. **18**(4): p. 046009.
46. Larkin, S., *Presumptive Field Testing Using Portable Raman Spectroscopy*, 2014.
47. Hazekamp, A., et al., *Chromatographic and spectroscopic data of cannabinoids from Cannabis sativa L.* Journal of liquid chromatography & related technologies, 2005. **28**(15): p. 2361-2382.
48. Bruker, *Differentiation of THC and CBD cannabis using FTIR.* 2019. **Application Note AN M157**: p. 1-3.
49. Mainali, D., *Quick and Real-Time Potency Determination of Cannabinoids Using FTIR Spectroscopy.* Aligent Technologies, Inc. , 2019: p. 1-4.
50. Lanzarotta, A., et al., *Hydrogen Bonding between Tetrahydrocannabinol and Vitamin E Acetate in Unvaped, Aerosolized, and Condensed Aerosol e-Liquids.* Analytical Chemistry, 2020. **92**(3): p. 2374-2378.
51. *LabRAM HR Evolution: Confocal Raman Microscope.* HORIBA. horiba.com/en_en/products/detail/action/show/Product/labram-hr-evolution-1083/
52. Yvon, H.J., *LabRAM User Guide: An Introduction to the Software and Hardware.* 2004: p. 56-58.
53. Kanchanakungwankul, S.B., J. L.; Zheng, J.; Alecu, I. M.; Lynch, B. J.; Zhao, Y.; Truhlar, D. G., *Database of Frequency Scale Factors for Electronic Model Chemistries.* 2018.
54. Borges, R., et al., *Understanding the Molecular Aspects of Tetrahydrocannabinol and Cannabidiol as Antioxidants.* Molecules (Basel, Switzerland), 2013. **18**: p. 12663-12674.